AGU PUBLICATIONS

JGR

Journal of Geophysical Research: Atmospheres

RESEARCH ARTICLE

10.1002/2014JD022468

Key Points:
- Good agreement of simulated age and trend with MIPAS observations
- Local residual circulation and mixing effects on mean age are opposite
- QBO strongly affects mean age interannual variability globally

Correspondence to:
F. Ploeger,
f.ploeger@fz-juelich.de

Citation:
Ploeger, F., M. Riese, F. Haenel, P. Konopka, R. Müller, and G. Stiller (2015), Variability of stratospheric mean age of air and of the local effects of residual circulation and eddy mixing, *J. Geophys. Res. Atmos.*, *120*, 716–733, doi:10.1002/2014JD022468.

Received 20 AUG 2014
Accepted 11 DEC 2014
Accepted article online 12 DEC 2014
Published online 19 JAN 2015

Variability of stratospheric mean age of air and of the local effects of residual circulation and eddy mixing

F. Ploeger[1], M. Riese[1], F. Haenel[2], P. Konopka[1], R. Müller[1], and G. Stiller[2]

[1]Institute of Energy and Climate Research, Stratosphere (IEK-7), Forschungszentrum Jülich, Jülich, Germany, [2]Institute for Meteorology and Climate Research, Karlsruhe Institute of Technology, Karlsruhe, Germany

Abstract We analyze the variability of mean age of air (AoA) and of the local effects of the stratospheric residual circulation and eddy mixing on AoA within the framework of the isentropic zonal mean continuity equation. AoA for the period 1988–2013 has been simulated with the Lagrangian chemistry transport model CLaMS driven by ERA-Interim winds and diabatic heating rates. Model simulated AoA in the lower stratosphere shows good agreement with both in situ observations and satellite observations from Michelson Interferometer for Passive Atmospheric Sounding, even regarding interannual variability and changes during the last decade. The interannual variability throughout the lower stratosphere is largely affected by the quasi-biennial-oscillation-induced circulation and mixing anomalies, with year-to-year AoA changes of about 0.5 years. The decadal 2002–2012 change shows decreasing AoA in the lowest stratosphere, below about 450 K. Above, AoA increases in the Northern Hemisphere and decreases in the Southern Hemisphere. Mixing appears to be crucial for understanding AoA variability, with local AoA changes resulting from a close balance between residual circulation and mixing effects. Locally, mixing increases AoA at low latitudes (40°S–40°N) and decreases AoA at higher latitudes. Strongest mixing occurs below about 500 K, consistent with the separation between shallow and deep circulation branches. The effect of mixing integrated along the air parcel path, however, significantly increases AoA globally, except in the polar lower stratosphere. Changes of local effects of residual circulation and mixing during the last decade are supportive of a strengthening shallow circulation branch in the lowest stratosphere and a southward shifting circulation pattern above.

1. Introduction

The global stratospheric circulation, termed the Brewer-Dobson (BD) circulation [*Brewer*, 1949; *Dobson et al.*, 1929], plays a key role for the global transport of trace gases and for related effects on chemistry and radiation. From a two-dimensional point of view the BD circulation consists of a residual mean meridional mass circulation ("residual circulation," in the following), causing upward cross-isentropic transport of air in the tropics and downward transport in the extratropics and of additional isentropic (quasi-horizontal) mixing by large-scale eddies ("eddy mixing") [e.g., *Plumb*, 2002]. The residual circulation is mechanically driven by breaking atmospheric waves [e.g., *Haynes et al.*, 1991]. Likewise, eddy mixing results from stirring related to wave breaking [e.g., *Haynes and Shuckburgh*, 2000a, 2000b]. Changes in the BD circulation cause changes in trace gas distributions which, in turn, may impact surface climate [e.g., *Solomon et al.*, 2010; *Riese et al.*, 2012]. Based on model simulations, the stratospheric circulation itself has been shown to change in response to increasing greenhouse gas concentrations [e.g., *Rind et al.*, 1990]. Current general circulation models (GCMs) consistently simulate an accelerating stratospheric residual circulation in a changing climate, as diagnosed from an increasing upward mass flux in the tropics [e.g., *Butchart et al.*, 2010]. Physical mechanisms causing this acceleration have been proposed, like enhanced wave driving forced by both increasing tropospheric temperatures and sea surface temperatures [e.g., *Garcia and Randel*, 2008; *Oberländer et al.*, 2013] and shifting critical levels for wave breaking [*Shepherd and McLandress*, 2011].

The mean age of air (AoA) of an air parcel in the stratosphere measures the average time elapsed since the air parcel had last contact with the well-mixed troposphere [e.g., *Hall and Plumb*, 1994]. Consequently, without mixing, an air parcel steadily ages on its pathway after entering the stratosphere across the tropical tropopause. Long-term changes of AoA are widely accepted as a proxy for changes in the residual circulation, with decreasing AoA reflecting an accelerating circulation. Current GCMs consistently simulate an AoA decrease throughout the global stratosphere [e.g., *Butchart et al.*, 2010]. Observationally based estimates of AoA, however, provide no indication for an accelerating stratospheric circulation. Instead, balloon-borne

measurements show a slightly positive AoA trend in the Northern Hemisphere (NH, Southern Hemisphere SH) subtropics and midlatitudes for the last 30 years [*Engel et al.*, 2009]. Moreover, global AoA estimates based on SF_6 satellite measurements by the Michelson Interferometer for Passive Atmospheric Sounding (MIPAS) instrument show a nonuniform pattern of AoA changes during the last decade (2002–2010), with a clear AoA increase in the NH subtropical and midlatitude stratosphere [see *Stiller et al.*, 2012, Figure 10].

Several studies have recently addressed the discrepancy between observations and models, regarding trends of stratospheric mean age of air. *Garcia et al.* [2011] pointed to the sparse sampling of balloon observations, which might render observed AoA trends less reliable than those from models. *Bönisch et al.* [2011] argued for a changing pattern of the BD circulation, with an increase in the shallow circulation branch and a moderate weakening in the deep circulation branch, which could explain AoA and ozone observations [*Ray et al.*, 2010]. However, the interpretation of observed AoA changes in terms of changes in the BD circulation remains a matter of current debate. In particular, the effect of mixing on AoA seems important [e.g., *Ray et al.*, 2010]. In general, increased mixing in the subtropical lower stratosphere causes a strengthening of recirculation into the tropics, increasing AoA [*Neu and Plumb*, 1999; *SPARC-CCMVal*, 2010]. In a very recent paper, *Garny et al.* [2014] further studied this effect and showed that the integrated effect of mixing along an air parcel's pathway through the stratosphere results in an additional aging throughout most of the stratosphere, which they termed "aging by mixing." However, none of these studies calculated the mixing effect explicitly. Consequently, they could not derive further mixing characteristics such as regional patterns, and many details of the mixing effect on AoA are still unknown.

In this paper, we simulate global stratospheric AoA with the Lagrangian chemistry transport model CLaMS (Chemical Lagrangian Model of the Stratosphere) [*McKenna et al.*, 2002] driven by European Centre for Medium-Range Weather Forecasts (ECMWF) ERA-Interim meteorological data for the period 1988–2013. We particularly focus on comparisons to the satellite observations from the MIPAS instrument, available during the last decade. Our aim is to investigate the variability of stratospheric mean age of air and of the local effects of the residual circulation and eddy mixing. Therefore, we separate the effects of the residual circulation and of mixing on simulated AoA by applying the isentropic zonal mean continuity equation, the equivalent isentropic formulation of the Transformed Eulerian Mean (TEM) framework [e.g., *Andrews et al.*, 1987]. Using this approach, we are able to explicitly calculate the local effect of eddy mixing on mean age of air and to analyze its regional patterns and temporal changes.

First, we compare simulated AoA to observations (section 2), finding good agreement for the mean age distribution, its interannual variability and even for its change during the last decade (2002–2012). Second, we analyze variability on seasonal up to interannual timescales. In particular, the quasi-biennial oscillation (QBO) [e.g., *Baldwin et al.*, 2001] turns out to be an important factor causing interannual variability of AoA throughout large parts of the stratosphere. Further, we investigate the temporal variability of the local effects of residual circulation versus mixing, and we analyze the (latitude/altitude) distribution of local mixing effects and their integrated impact on global AoA (sections 3 and 4). We note already here that the investigation of local effects of circulation and mixing allows no conclusions to be drawn about the integrated effect of mixing on the age of an air parcel, because AoA at a given location has been nonlocally influenced during its pathway through the stratosphere. These issues are further discussed in section 3. However, the local analysis allows exploring the nonuniform global patterns of the effects of residual circulation and mixing and hence provides local information about these processes and their decadal changes (section 5). In this sense, we discuss the changes of the local effects of residual circulation and eddy mixing and show that their decadal change during the 2002–2012 period is consistent with a strengthening shallow residual circulation branch in the lowest part of the stratosphere and a shifting circulation pattern above.

2. Age of Air Simulation and Observations

Mean age of air has been simulated with the Chemical Lagrangian Model of the Stratosphere (CLaMS) [*McKenna et al.*, 2002] for the period 1988–2013, after initialization from a monthly zonal mean climatology based on the MIPAS AoA observations of *Stiller et al.* [2008] and an 8 year spin-up period (with perpetual 1988 conditions). We ensured independence of our results from the initialization by carrying out an identical simulation for the 2002–2012 period and comparing the two simulations during this period, ensuring that both simulations produce comparable results. The Lagrangian transport of trace gases in CLaMS is based on three-dimensional air parcel forward trajectories and a parameterization of small-scale irreversible

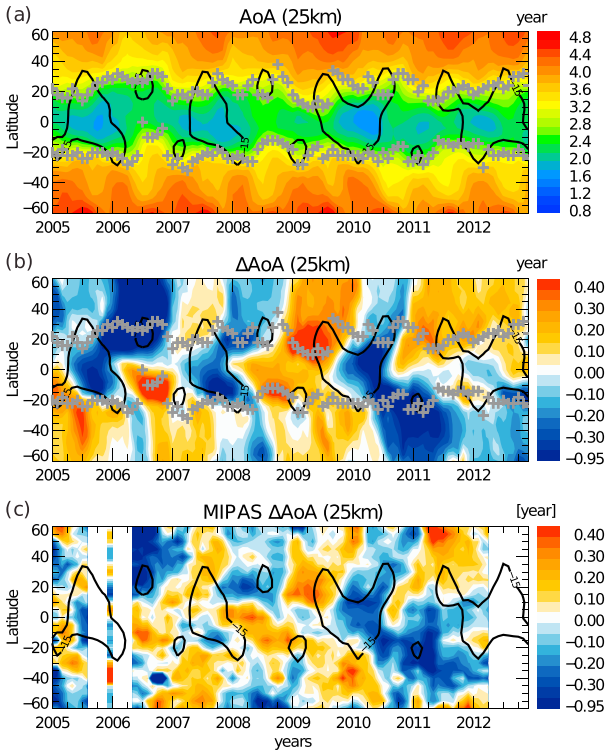

Figure 1. (a) Mean age of air (AoA) at 25 km from CLaMS simulation for 2005–2012 and corresponding deseasonalized anomalies (b) from CLaMS and (c) from MIPAS observations. (CLaMS AoA has been averaged between 22 and 28 km.) Black line shows easterly zonal wind (−15 m/s), gray symbols show the subtropical transport barrier, determined from the minima in the monthly mean age probability distribution functions (see text).

mixing induced by deformations in the large-scale atmospheric flow [*Konopka et al.*, 2004]. The model is driven with meteorological data from the ECMWF ERA-Interim reanalysis [*Dee et al.*, 2011]. Throughout the stratosphere (above about 300 hPa) potential temperature θ is used as vertical coordinate in the model, and vertical cross-isentropic velocity is deduced from the ERA-Interim forecast total diabatic heating rate [*Ploeger et al.*, 2010].

The Lagrangian transport model CLaMS has been shown to simulate the global stratospheric trace gas distributions well and even the small-scale structures and steep gradients therein [e.g., *Konopka et al.*, 2004]. In particular, the multi-year simulation analyzed here has been shown to realistically represent transport of ozone and water vapor in the lower stratosphere [e.g., *Konopka et al.*, 2010; *Ploeger et al.*, 2013]. The mean age of air in the model is calculated from a "clock tracer" [e.g., *Hall and Plumb*, 1994; *Waugh and Hall*, 2002], a synthetic species with linearly increasing mixing ratio in the lowest model layer (orography following) and without any sources or sinks above. For further details about this multiyear CLaMS simulation, see *Pommrich et al.* [2014].

Mean age of air is not directly measurable but may be estimated from measurements of long-lived trace gas species with approximately linearly increasing mixing ratios in the troposphere [*Hall and Plumb*, 1994]. MIPAS AoA is deduced from observations of SF_6, as described in much detail by *Stiller et al.* [2008, 2012]. The data version shown here is an improved data record of MIPAS age of air, derived from more recent version 5 spectral data with further improvements in the retrieval setup. It covers the full MIPAS mission lifetime from 2002 to 2012. For more details on this data record, see *Haenel et al.* [2014]. The vertical resolution is about 4–6 km around 20 km altitude and degrading at higher levels (e.g., 7–10 km around 30 km). Major uncertainty of SF_6 based AoA estimates occurs at high latitudes and is related to the mesospheric sink of SF_6, causing a high bias in deduced AoA (compare Figure A1). Note that a systematic error related to non-LTE effects (on the order of 0.5 year), as discussed by *Stiller et al.* [2008], has been corrected in the new retrieval version used here.

Figure 1a shows AoA at 25 km from the CLaMS simulation for the period 2005–2012. To account for the coarse vertical resolution of MIPAS AoA data we averaged the model AoA between about 22–28 km, for the comparison in Figure 1. The simulation shows a strong horizontal AoA gradient in the subtropics, which appears in distributions of other long-lived trace gas species as well, and which is indicative for a barrier to horizontal transport between the tropics and midlatitudes at these altitudes [e.g., *Plumb*, 1996]. A certain part of the AoA variability is caused by the annual cycle and its hemispheric asymmetries. Here we focus mainly on interannual variability. In the tropics, a clear oscillating signal emerges with a period of about 2 years, linked to the QBO, with minimum AoA occurring during QBO easterly phase (black contours show easterly zonal wind). The QBO induces a secondary meridional circulation leading to enhanced tropical upwelling during QBO easterly shear phases and further shifts the subtropical mixing barriers [e.g., *Baldwin et al.*, 2001; *Punge et al.*, 2009]. The QBO-induced circulation anomalies result in anomalies in mixing ratios

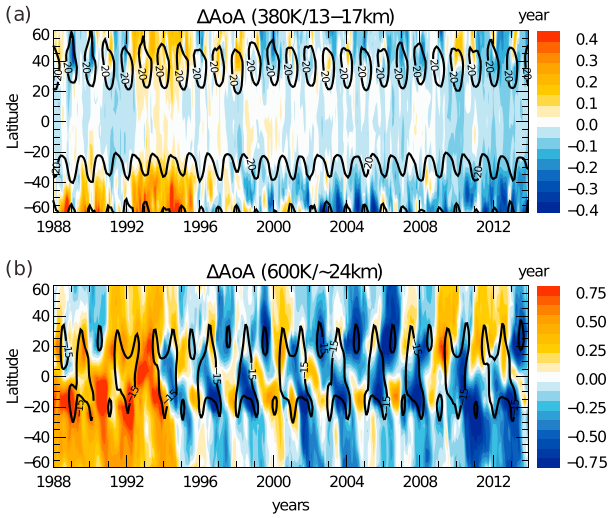

Figure 2. Mean age of air (AoA) deseasonalized anomalies at (a) 380 K (~13–17 km) and (b) 600 K (~24 km) from CLaMS simulation for 1988–2013. Black lines show zonal wind contours (20 m/s at 380 K and −15 m/s at 600 K).

of long-lived trace gases [e.g., *Randel et al.*, 1998]. The youngest tropical AoA during QBO easterly phases in Figure 1a is consistent with the enhanced upwelling induced by the secondary meridional circulation (further discussion in section 4).

Figures 1b and 1c further show deseasonalized anomalies (after subtracting the mean annual cycle) of AoA at the same altitude (25 km) from the CLaMS simulation and from MIPAS observations. We compare anomalies because these are most suitable for investigating temporal variability, which is the focus of this paper. Note that the effect of the mesospheric SF_6 sink likely causes a high bias of SF_6-based AoA estimates and an offset between CLaMS and MIPAS AoA, particularly at high latitudes (see discussion above and Appendix A). The anomalies globally show a pattern of repeating minima and maxima with a period of about 2 years, related to the QBO, as already observed for the unfiltered time series. Although the measurement-based distribution appears more patchy than the simulation, there is good agreement between the model simulation and MIPAS for both the pattern and magnitude of the anomalies. In addition, we find good agreement between the CLaMS simulation and mean age estimates based on various in situ observations at 20 km (see Appendix A), enhancing the confidence in the CLaMS simulated mean age.

Closer inspection of the anomaly pattern reveals that maximum anomalies occur in the subtropics. We estimated the location of the subtropical transport barrier (gray symbols), following the method described by *Sparling* [2000]. Therefore, the hemispheric probability distribution functions (pdfs) of simulated mean age for the respective level have been constructed for all months of the considered period. The minimum of the pdf indicates the mean age value at the transport barrier, from which the corresponding barrier latitude can be derived (for details, see *Sparling* [2000]). The transport barrier latitude shows a distinct undulation, consistent with the findings of *Palazzi et al.* [2011] of a wintertime shift of the subtropical barrier toward the summer hemisphere during QBO westerly phase. This undulation of transport barrier location results from the shift of the zero wind line toward the summer hemisphere during QBO westerly phase, allowing planetary waves and associated mixing to penetrate to lower latitudes compared to easterly phase [*Holton and Tan*, 1980; *Gray and Russell*, 1999]. The AoA distribution responds to the combined effects of the QBO-related meridional circulation and mixing modulation [e.g., *Gray and Russell*, 1999; *Choi et al.*, 2002], with QBO westerlies coinciding with anomalously weak tropical upwelling and enhanced extratropical isentropic stirring [*Shuckburgh et al.*, 2001]. As a consequence, maximum positive AoA anomalies occur in the wintertime subtropics during QBO westerly phase (e.g., winter 2008/2009). Remarkably, the QBO-induced anomalies clearly affect the AoA variability even at extratropical latitudes. Related year-to-year differences frequently amount to about 0.5 year.

In Figure 2, deseasonalized anomalies of AoA from the CLaMS simulation are shown at 380 K (ranging from ~13 km at high latitudes to ~17 km in the tropics) and at 600 K (~24 km), for the full simulation period 1988–2013. Both levels show anomalously old air before about 1995, which is likely in parts related to the eruption of Mount Pinatubo in June 1991 [e.g., *Diallo et al.*, 2012]. We exclude this period of anomalously old air from the following analysis and focus on AoA variability during the last decade (2002–2013). In the lowermost stratosphere at 380 K, AoA variability is dominated by the annual cycle, and hence, the deseasonalized anomaly shows no clear periodic signal. The anomalies maximize in the extratropics, whereas at higher levels (e.g., 600 K, see Figure 2b) they maximize more in the subtropics due to the QBO-related transport barrier modulation (see above). The decadal change of AoA from about 2000 to 2013 at 380 K shows a decrease, which appears to be clearest at lower latitudes.

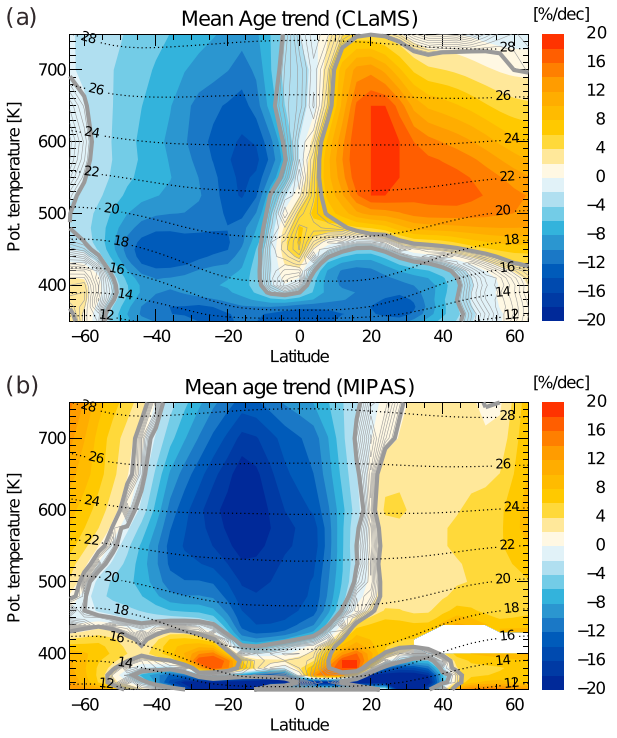

Figure 3. Relative decadal change (in percent) of zonal mean age of air for the period 2002–2012 from (a) CLaMS and (b) MIPAS, calculated from a linear regression. The significance of the linear trend, measured in multiples of the standard deviation σ, is shown as gray contours (2 σ contour as thick, then decreasing with 0.2 step as thin lines). Dashed lines show altitude levels in kilometers. The MIPAS data have been adapted from *Haenel et al.* [2014].

At 600 K, the AoA anomalies show the QBO-related oscillation already noted above. However, the figure shows additional modulation with much stronger anomalies during particular periods (e.g., after 2008). The decadal change from about 2000 to 2013 at 600 K shows a clear difference between the two hemispheres, with an AoA decrease in the SH and an AoA increase in the NH. Figure 2b further shows that this particular pattern is not representative for a long-term trend, but largely affected by the anomalously old air in the NH and anomalously young air in the SH after about 2008, likely related to decadal variability. The anomalously old air in the NH after 2008 is even visible in the lowermost stratosphere at 380 K (Figure 2a).

Satellite-based measurements by the MIPAS instrument provide the only global observationally based data set of mean age trends hitherto [*Stiller et al.*, 2012; *Haenel et al.*, 2014]. Clearly, the measurement period of MIPAS (2002–2012) is rather short, and respective AoA changes are likely affected by decadal variability. The global pattern of the relative decadal AoA change (calculated as linear trend, after deseasonalizing the AoA time series) for the 2002–2012 period simulated by CLaMS shows similar structures as observed by MIPAS (Figure 3). In particular, a clear decrease of AoA in the SH and an increase of AoA in the NH stratosphere emerge from both data sets. In these regions the linear trends in both data sets are significant on the 2 σ level (with σ the standard deviation of the linear trend and significance levels in multiples of σ shown as gray contours in Figure 3). Although the magnitude of simulated and observed decadal AoA changes differs, with the NH AoA increase stronger in the model and the SH AoA decrease stronger in the observations, the NH/SH increase/decrease pattern shows reliable agreement between model and observations. Note that the sign reversal of the decadal change occurs close to the equator in CLaMS, but displaced into NH subtropics in MIPAS (Figure 3). The cause for this difference is not clear. The difference south of 50°S is likely due to the existence of the mesospheric SF_6 sink (see above). We emphasize here that measuring as well as simulating AoA long-term changes is very challenging. In general, neither different models nor different observations agree exactly in their estimates, and differences between model trends and observations can be much larger and may even differ in their signs [e.g., *Waugh*, 2009]. We therefore consider the similarity between the CLaMS simulated decadal change pattern and MIPAS observations an encouraging result.

Closer inspection of Figure 3, shows a change in the evolution of simulated AoA at around 450 K. Above, AoA has increased in the NH and decreased in the SH, as discussed above. Below 450 K on the contrary, in particular, close to the tropopause, AoA has decreased during the last decade. Note that the comparison between CLaMS and MIPAS also shows inconsistencies in certain regions. For instance, the AoA decrease extends to higher altitudes in CLaMS, while MIPAS AoA increases in the subtropics in a layer around 400 K. However, the different evolution of simulated AoA below and above about 450 K indicates that different processes are likely to be involved, which will be further discussed in section 5.

3. Separation of Residual Circulation and Mixing Effects on Mean Age

A powerful diagnostic tool for investigating time variability of trace gases in the stratosphere is the Transformed Eulerian Mean (TEM) formalism [e.g., *Andrews et al.*, 1987]. To analyze the simulated age of air distributions, we use the equivalent approach for potential temperature θ as the vertical coordinate, based on the isentropic zonal mean continuity equation for trace gas mixing ratio χ [e.g., *Andrews et al.*, 1987, equation (9.4.21)]

$$\partial_t \overline{\chi} = S - \frac{\overline{v}^*}{a}\partial_\phi \overline{\chi} - \overline{Q}^* \partial_\theta \overline{\chi} + \frac{1}{\overline{\sigma}}\left[\nabla \cdot M - \partial_t(\overline{\sigma'\chi'})\right] . \quad (1)$$

The notation here follows *Andrews et al.* [1987], with overbars indicating zonal means and primes the deviations from these (fluctuations). The quantity $\sigma = -g^{-1}\partial_\theta p$ is the density in isentropic coordinates with p pressure and g the acceleration due to gravity. The ∇ operator is the gradient in the meridional plane, a is the Earth's radius, ϕ is latitude, and $\overline{v}^* = (\overline{\sigma v})/\overline{\sigma}$ and $= (\overline{\sigma Q})/\overline{\sigma}$ represent mass-weighted meridional and vertical wind velocities, with the cross-isentropic vertical velocity $\dot{\theta} = Q$. The first term S on the right-hand side of equation (1) represents chemical sources and sinks. The second and third terms contain the effects of horizontal and vertical advective transport by the diabatic residual circulation $(\overline{v}^*, \overline{Q}^*)$. The last term contains the eddy mixing effects, with the horizontal and vertical components of the eddy flux vector M given by $M_\phi = -\overline{(\sigma v)'\chi'}$ and $M_\theta = -\overline{(\sigma Q)'\chi'}$. Compared to the usual TEM framework, in the isentropic formulation an additional transient term $\partial_t(\overline{\sigma'\chi'})$ appears on the right-hand side of equation (1). Note that in isentropic coordinates the zonal mean tracer continuity equation is an exact equation, without neglecting higher-order terms.

Mean age of air Γ is given as the time lag between the stratospheric (χ) and tropospheric (χ^T) "clock tracer" mixing ratios $\chi(t) = \chi^T(t-\Gamma) = \gamma \cdot (t-\Gamma)$ [*Hall and Plumb*, 1994], with γ the constant tropospheric increase rate. Using this property and the fact that for the idealized model "clock tracer" $S = 0$, equation (1) induces an equation for the tendency (time derivative) of mean age of air [e.g., *Plumb*, 2002]

$$\partial_t \overline{\Gamma} = \left[1 - \frac{\overline{v}^*}{a}\partial_\phi \overline{\Gamma} - \overline{Q}^* \partial_\theta \overline{\Gamma}\right] + \frac{1}{\overline{\sigma}}\left[\nabla \cdot M^\Gamma - \partial_t(\overline{\sigma'\Gamma'})\right] . \quad (2)$$

Equation (2) shows that mean age of air fulfills a continuity equation like the mixing ratio of a passive tracer but with an additional unit source reflecting the fact that air ages by 1 year per year, while being transported through the stratosphere. For the sake of simplicity, we add the unit source to the advective terms and denote the sum of all three terms in the first square brackets on the right-hand side of equation (2) "residual circulation tendency" (or "local residual circulation effect"). The eddy flux vector components for mean age are given by $M^\Gamma_\phi = -\overline{(\sigma v)'\Gamma'}$ and $M^\Gamma_\theta = -\overline{(\sigma Q)'\Gamma'}$. The transient term $\partial_t(\overline{\sigma'\Gamma'})$ is very small and negligible for all results obtained in this paper (not shown). For the following, we include it into the eddy mixing tendency, for simplicity, and define the "mixing tendency" (or "local mixing effect") as

$$\mathcal{M} = \frac{1}{\overline{\sigma}}\left[\nabla \cdot M^\Gamma - \partial_t(\overline{\sigma'\Gamma'})\right] . \quad (3)$$

While the left-hand side of the mean age continuity equation (2) can be directly calculated from the AoA time series (hereafter directly calculated tendency), the right-hand side represents an indirect calculation of AoA tendencies resulting as the sum of the contributions from the residual circulation and eddy mixing (hereafter indirectly calculated tendency).

Model simulations provide all necessary quantities to evaluate equation (2), in particular, AoA values and their fluctuations as well as meteorological wind and temperature data on the same regular grid. Mean June AoA tendencies for the 2002–2012 time period are shown in Figure 4. The tendencies shown in Figure 4a are directly calculated from CLaMS AoA output fields and correspond to the left-hand side of equation (2). For comparison, Figure 4b displays tendencies that are indirectly calculated from the sum of all terms on the right-hand side of equation (2), including the contributions of residual circulation and eddy mixing. Overall, there is a remarkably good agreement between both terms throughout the stratosphere (similarly for all other months), which is a prerequisite for a meaningful diagnosis of simulated AoA variability based on the isentropic zonal mean formalism. In particular, during spring and summer (here June), AoA decreases in the NH lower stratosphere below about 500 K as a result of the "flushing" of this region with young air from low

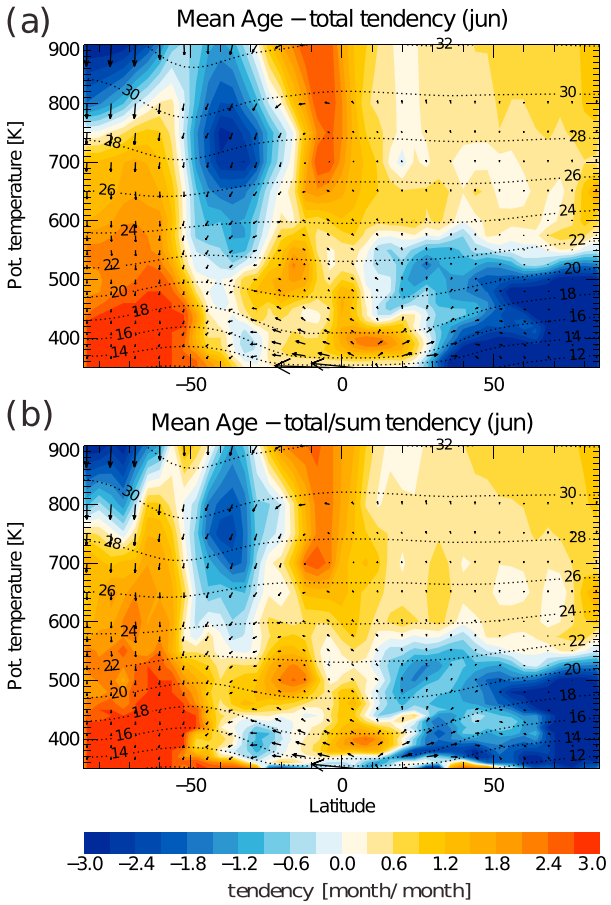

Figure 4. Mean June AoA tendency (2002–2012) calculated (a) directly as the time derivative of daily AoA time series and (b) indirectly as the sum of residual circulation and eddy mixing contributions, corresponding to the left-hand side and right-hand side of equation (2), respectively. Altitude levels (in km) are shown as dashed, the residual circulation as arrows.

latitudes [e.g., *Bönisch et al.*, 2008]. Above about 500 K, NH AoA increases during summertime. The strongest AoA increase during June, however, occurs in the SH extratropics due to diabatic descent in the Antarctic polar stratosphere.

3.1. Local Circulation and Mixing Effects and Relation to Circulation Patterns

We particularly emphasize the notation of the different tendencies in equation (2) as *local effects* on AoA. This highlights the fact that locally the AoA tendency, and hence the AoA variability, is controlled by the residual circulation and mixing tendencies at the given location, in the sense of equation (2). However, as recently pointed out by *Abalos et al.* [2013a] this local Eulerian view does not allow the air parcel history to be analyzed. Consequently, the AoA variability may be locally dominated by the residual circulation effect, while mixing has affected the air parcel earlier on its pathway and, indeed, is important for its composition [see, e.g., *Garny et al.*, 2014]. On the other hand, the clear advantage of the local (Eulerian) view is that it provides information about the local processes of residual circulation and mixing, which will be exploited in the following. In section 3.2 we further discuss the nonlocal (or integrated) effects of mixing on mean age. It is important to keep in mind that both the local and nonlocal (integrated) analysis provide complementary views of the same processes.

Figure 5 shows the local effects of the residual circulation and eddy mixing on mean AoA, averaged over the period 2002–2012. Both effects are diagnosed within the isentropic zonal mean framework of equation (2) as the respective contributions to the AoA tendency budget. The sum of both terms shown in the figure constitutes the (indirectly calculated) net AoA tendency.

In the tropics and subtropics, the local residual circulation effect decreases AoA on average by advecting young air masses upward and poleward. In the same region, eddy mixing increases AoA by in-mixing of aged air from high latitudes. At middle and high latitudes the residual circulation increases AoA by downward advection of aged air from above, whereas eddy mixing decreases AoA by horizontal (isentropic) exchange with the tropics. Therefore, mixing locally counteracts the effect of advection by the residual circulation. As a consequence, both local effects of residual circulation and mixing on AoA largely cancel throughout the global stratosphere. Observable AoA changes locally emerge as the residual from this balance. Under steady state conditions (e.g., for an annual mean atmosphere in the absence of trends) a total cancelation could have been expected from the mean balance between local residual circulation and eddy mixing effects in equation (2). An approximate cancelation holds also for individual seasons, and has already been demonstrated for stratospheric trace gas species like N_2O [*Randel et al.*, 1994], again illustrating the tracer-like character of mean age.

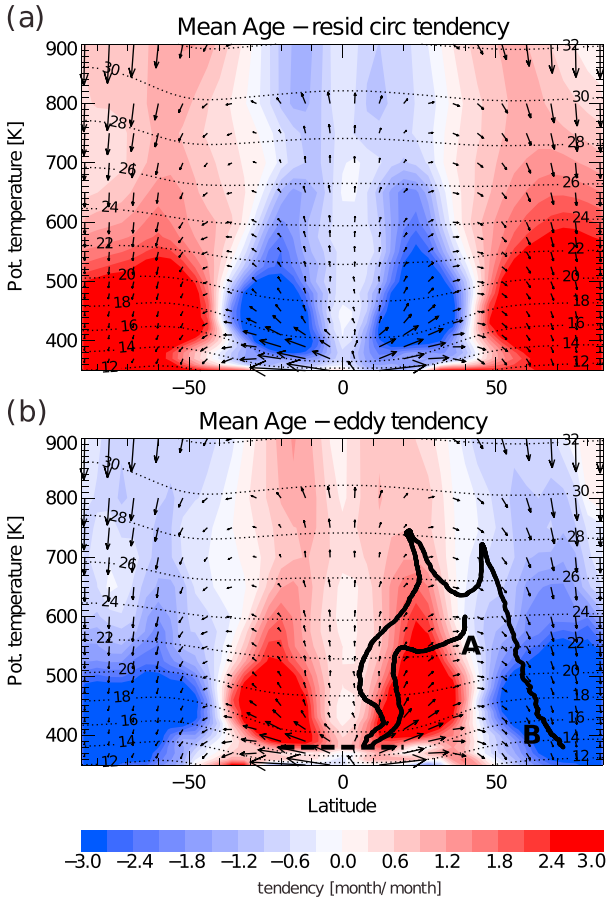

Figure 5. Contributions of (a) residual circulation and (b) eddy mixing to the mean age tendency budget (2002–2012 average), deduced from the isentropic AoA continuity equation (2). Thick black lines show two residual circulation trajectories starting at 40°N/600 K (A) and 72°N/380 K (B), respectively (thick dashed line shows 380 K isentrope, see section 3.2 for details). Altitude levels are shown as dashed, residual circulation as arrows.

Comparison of the local residual circulation and eddy mixing effects on AoA in Figure 5 illustrates how both effects contribute to the poleward transport of young air. This poleward transport is caused by advection by the residual circulation equatorward of about 40° and by eddy mixing poleward. Recently, *Ploeger et al.* [2013] found a similar latitudinal separation for the local effects of residual circulation and eddy mixing on horizontal water vapor transport. The enhanced vertical gradient in the local residual circulation effect around 500 K (~20 km) and the strong horizontal gradient around 40°N/S indicate the separation of a shallow circulation branch from the deep branch above [compare *Birner and Bönisch*, 2011]. The sign reversal in the local residual circulation and mixing effects around 40°N/S shows the latitudinal separation between both circulation branches. Equatorward of about 40°N/S, advection by the shallow branch transports air from the tropics poleward. At higher latitudes (poleward of about 40°N/S) downward advection of old air from above by the deep branch dominates the residual circulation effect (see Appendix B for a separation between vertical and horizontal tendency components), resulting in the separation of aspect ratios, the ratios of vertical to meridional extent of air parcel trajectories, as shown by *Birner and Bönisch* [2011]. The strong vertical gradients in the climatological mean of both effects around 500 K are, to some degree, related to a different seasonality in the deep and shallow circulation branches.

3.2. Nonlocal (Integrated) Mixing Effect: "Aging by Mixing"

Remarkably, strongest local eddy mixing occurs below about 500 K (Figure 5). However, this fact by no means implies that mixing is unimportant for AoA above. It has been shown that stronger mixing increases recirculation into the tropics and increases AoA [e.g., *Neu and Plumb*, 1999; *Strahan et al.*, 2009; *SPARC-CCMVal*, 2010]. Recently, *Garny et al.* [2014] pointed out that mixing between tropics and extratropics in the lowest part of the stratosphere crucially affects AoA at all levels above the mixing level, causing an additional aging. They diagnosed the effect of mixing as the difference between simulated AoA and the transit time along the residual circulation and denoted this difference as "aging by mixing." Our approach based on the zonal mean tracer continuity equation offers the facility to calculate this "aging by mixing" explicitly. For that purpose, equation (2) has to be integrated along a residual circulation trajectory ending at a given location and time t (a characteristic of equation (2)), which is the path followed by this air parcel if it were advected by the residual circulation. Along this trajectory, $\mathrm{d}/\mathrm{d}t = \partial_t + \frac{\overline{v}^*}{a}\partial_\phi + \overline{\mathrm{Q}}^*\partial_\theta$, and equation (2) yields an equation for mean age at that location and time.

$$\overline{\Gamma}(t) = \tau_{\,\mathrm{RCTT}} + \int_{t_0}^{t} \mathcal{M}\,\mathrm{d}t' \,. \tag{4}$$

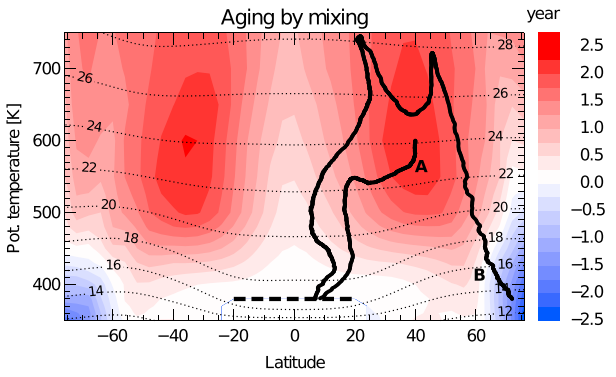

Figure 6. "Aging by mixing," diagnosed as the nonlocal effect of eddy mixing on mean age integrated along residual circulation trajectories (see text), as average for 2002–2012. Thick black lines show two residual circulation trajectories starting at 40°N/600 K (A) and 72°N/380 K (B), respectively (thick dashed line highlights tropical tropopause at 380 K).

The first term on the right-hand side is the residual circulation transit time $\tau_{RCTT} = t - t_0$, with t_0 the time of tropopause crossing. The second term, the integrated local mixing effect, represents the additional aging by mixing. Consequently, equation (4) provides a separation of mean age into the integrated effects of advection by the residual circulation and mixing along the residual circulation trajectory.

To diagnose the aging by mixing using equation (4), we start backward trajectories along a regular latitude/θ grid every fifteenth of each month from 2002 to 2012. Trajectories are calculated backward using the daily mean residual circulation velocities ($\overline{v}^*, \overline{Q}^*$), until they cross the 380 K surface between 20°N/S (representative of the tropical tropopause). Finally, the daily local mixing tendencies are integrated along these trajectories, in a forward sense, resulting in the (integrated) aging by mixing.

Figure 6 clearly shows that the nonlocal effect of mixing, integrated along the residual circulation trajectories, causes an additional aging throughout most of the stratosphere, in good agreement with the results of *Garny et al.* [2014, Figure 2]. Maximum aging by mixing occurs in the subtropical and midlatitude stratosphere above about 20 km, with a maximum additional aging of about 2 years. Only in the lower polar stratosphere mixing results in a decrease of mean age. The pattern of the local mixing effect clearly shows the reason for this decrease (Figure 5b). The air parcel ending within the subtropical region of maximum integrated mixing effect (black line, labeled A) samples only regions of positive local mixing tendencies. In contrast, the air parcel ending within the region of negative integrated mixing effect (B) samples atmospheric regions of totally different mixing characteristics. This air parcel is strongly affected by the negative local mixing tendencies at high latitudes (Figure 5b) and less by the large positive mixing tendencies in the subtropics, such that the net integrated mixing effect (aging by mixing) is negative.

We emphasize again that our approach to diagnose the additional nonlocal aging by mixing is based on an exact calculation of daily local eddy mixing tendencies. Therefore, the calculated aging by mixing is not influenced by additional numerical uncertainties and diffusion in the model.

4. Variability in Mean Age and in Local Residual Circulation and Mixing Effects

To investigate the variability in residual circulation and mixing at a given location, analysis of their local effects is required. In particular, regarding variability on shorter timescales (here seasonal to interannual), this provides a valid method to quantify the impact of the local residual circulation and mixing, which has been extensively used for many different trace gas species [e.g., *Randel et al.*, 1994, 1998; *Abalos et al.*, 2013b]. As pointed out above (section 3.2), the local analysis constitutes a complementary view to the nonlocal, integrated approach, with both methods yielding consistent results (see Figure 6). In this section, we discuss the variability from seasonal to interannual timescales in more detail and for four different regions, in the tropical, the NH subtropical, the polar, and within the lowermost stratosphere.

4.1. Tropical Stratosphere

Figure 7a relates the AoA variability in the tropical stratosphere at 600 K (about 24 km) to the local effects of residual circulation and eddy mixing, using the framework of equation (2). The figure shows the time series of AoA (top), directly and indirectly calculated AoA tendencies (middle) and the contributions of residual circulation and eddy mixing to the tendency (bottom). The variability of the AoA time series results from the superposition of different frequencies (e.g., annual cycle and QBO). Comparison of the directly calculated net AoA tendency to the net tendency indirectly calculated by summing up all terms on the right-hand side of equation (2) shows that the calculated budget is very well closed (black versus orange lines in Figure 7a, middle). Hence, our calculation is consistent and includes all significant contributions.

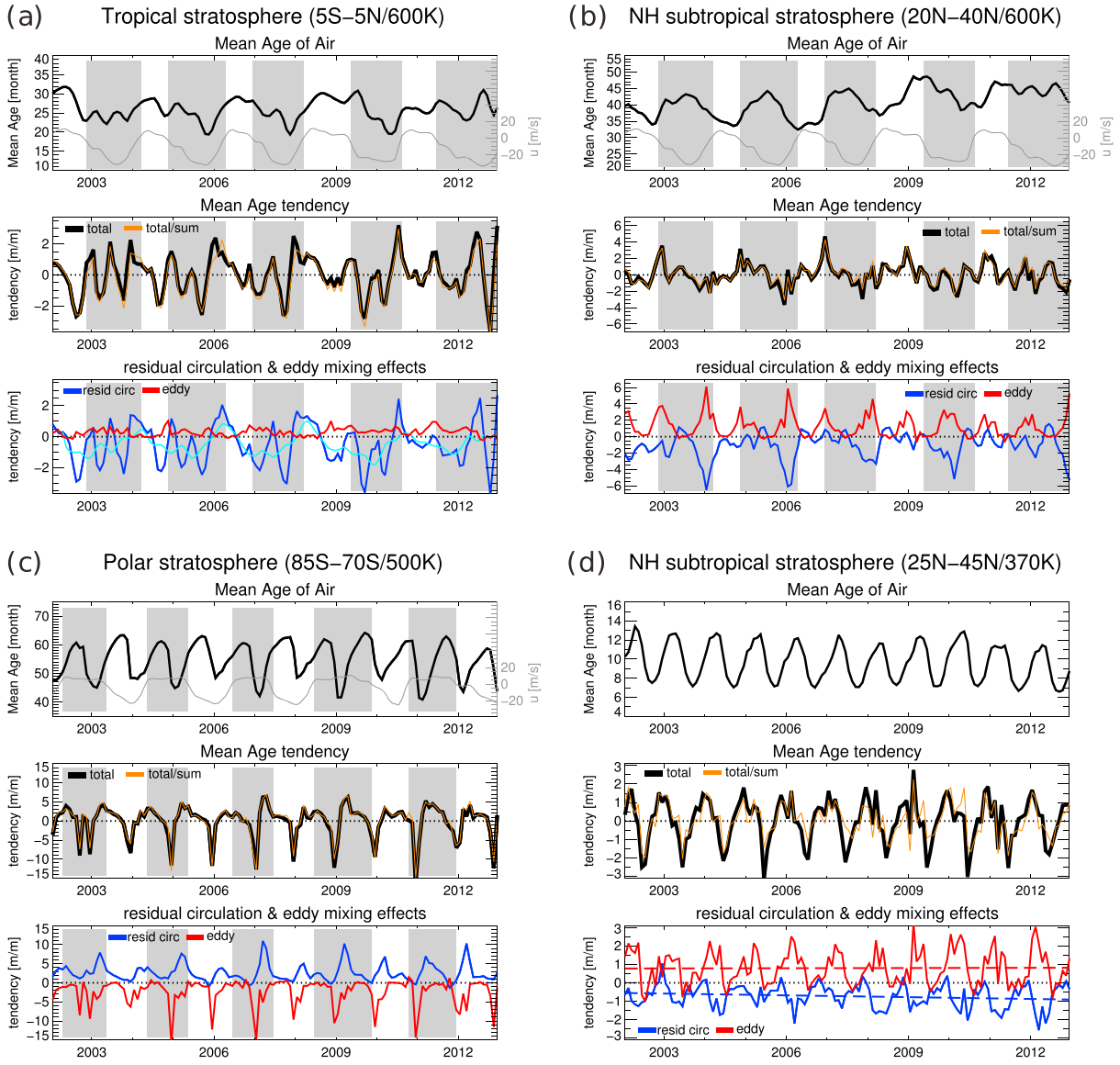

Figure 7. (a) Mean age time series (2002–2012) in the tropical stratosphere (600 K, 5°S–5°N) from CLaMS (top), the directly and indirectly calculated net tendencies (black and orange, middle), and the contributions to the tendency due to local residual circulation and eddy mixing (blue and red, bottom). The gray line shows the tropical (10°S–10°N) zonal wind at the given level, the gray shading highlights the corresponding QBO easterly phases (top). The same analysis is shown for (b) the NH subtropical stratosphere, (c) the SH polar stratosphere, and (d) the NH lowermost stratosphere. The light blue line in Figure 7a (bottom) shows the local circulation effect smoothed with a 6 month running mean. Red and blue dashed lines in Figure 7d show linear trends of the effects, black dotted lines show the base line.

The comparison of the different tendencies in Figure 7a (bottom) shows that in the tropics, locally the residual circulation effect clearly dominates (residual circulation tendency, blue), whereas the mixing effect almost vanishes (mixing tendency, red). The variability of the net AoA tendency (Figure 7a, middle), resulting from the superposition of both effects, clearly follows the residual circulation. Each increase or decrease of AoA during the considered period is caused locally by the residual circulation (e.g., compare the coinciding maxima in winters 2006 and 2008 or in summers 2010 and 2012 in the net tendency and in the residual circulation tendency). We emphasize again that this strong dependence of tropical AoA variability on the residual circulation by no means implies that mixing is unimportant for AoA in the tropics. Remote mixing processes may significantly affect AoA even at locations where the local tendency is dominated by the residual circulation (compare Figure 6). Locally, however, the tropical AoA variability on seasonal to interannual timescales can be largely anticipated from the local variability of the residual circulation.

The tropical AoA time series in Figure 7a is clearly modulated by the QBO. Figure 7a shows that AoA decreases occur during QBO easterly shear phases when tropical upwelling modulated by the QBO is strongest, for instance, during winters 2005/2006 and 2007/2008, and during spring 2009 (QBO easterly phases at the respective level are shaded in gray in Figure 7, the mean zonal wind between 10°S and 10°N at the considered level is shown as a gray line). The residual circulation effect in Figure 7a (bottom), smoothed with a 6 month running mean (light blue), clearly illustrates that these AoA decreases are related to the enhanced upwelling during QBO easterly shear phases.

4.2. NH Subtropical Stratosphere

In the NH subtropical stratosphere (Figure 7b), the clearest signal in the AoA time series is the approximately 2 year oscillation related to the QBO. However, the attribution of subtropical AoA minima and maxima to particular QBO phases (which are defined by winds in the deep tropics) is less clear than in the tropics. The AoA minima mainly occur at the end of QBO easterly phases (in 2004 even in the westerly phase), while the maxima occur at the end of westerly phases.

As already stated in section 2, the QBO induces a secondary meridional circulation and modulates mixing [e.g., *Baldwin et al.*, 2001]. As a result, the subtropical transport barriers shift toward the summer hemisphere during QBO westerly phase [e.g., *Palazzi et al.*, 2011], caused by a weakened meridional circulation and planetary waves penetrating to lower latitudes (shift of zero wind line). The local effect of eddy mixing to the AoA tendency is largely opposite to the local residual circulation effect (Figure 7b (bottom), and the net AoA variability results as the residual of these two opposite effects. Both local effects show a clear modulation by the QBO, maximizing at the end of QBO easterly phase. The modulation of the local residual circulation effect appears stronger, such that during westerly phase to easterly shear phase the local mixing effect dominates and AoA increases. This is consistent with the shift of transport barriers toward the summer hemisphere during westerly phase (compare Figure 1). During these periods (e.g., during winters 2005/2006, 2006/2007, and 2008/2009) the transport barrier is located equatorward of the subtropics, such that poleward advection of young tropical air by the residual circulation is strongly suppressed and mixing may increase AoA.

Closer inspection of the time series of local circulation and mixing effects in Figure 7b (bottom) shows a weakening of both effects in the subtropics during the last decade. This decadal change of the local effects will be further discussed in section 5.

4.3. Polar Stratosphere

In the SH polar stratosphere (here 500 K) AoA shows a distinct annual cycle with oldest air at the end of austral winter (Figure 7c), related to strong isolation within the polar vortex and downwelling of aged air from above due to diabatic descent. Again, the local effects of the residual circulation and eddy mixing are opposite, with the circulation effect increasing AoA and the mixing effect decreasing AoA. Compared to the subtropical latitudes (Figure 7b), in the polar stratosphere the maximum residual circulation and eddy mixing effects are slightly displaced in time and therefore the resulting net AoA changes turn out to be much larger.

The AoA decrease at the end of winter occurs very abruptly every year when the vortex breaks up and lasts for only about a month. The corresponding large negative net tendencies decreasing AoA in spring (Figure 7b, middle) can be clearly attributed to eddy mixing (Figure 7b, bottom), mixing in younger air masses from midlatitudes. The year 2002 of the Antarctic vortex split [e.g., *Newman and Nash*, 2006] shows an anomalous behavior with two consecutive (negative) peaks in eddy mixing, likely related to the split and the final vortex breakup.

During austral fall and winter, downwelling because of the residual circulation steadily increases AoA at polar latitudes. Note that the residual circulation effect shows a clear modulation with weaker aging during QBO easterly shear phases (QBO phases in Figure 7c have been defined at 500 K, whereas in Figures 7a and 7b they have been defined at 600 K). This illustrates how the QBO may affect even polar latitudes via modulating wave propagation, wave breaking, and the resulting downwelling [e.g., *Holton and Tan*, 1980].

4.4. Lowermost Stratosphere

Within the lowermost stratosphere (370 K), the clearest AoA variability appears to be related to the annual cycle [see also *Bönisch et al.*, 2008], with oldest air during winter and youngest air at the end of summer (Figure 7d). The local effects (bottom) show how the "flushing" of the NH with young air during spring and summer (negative net tendencies in Figure 7d, middle) is locally related to the superposition of residual

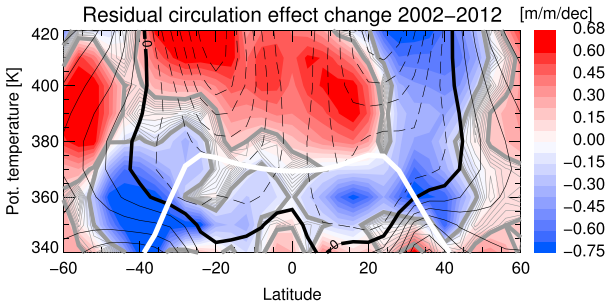

Figure 8. Decadal change (2002–2013) of local residual circulation tendency on mean age (color shading), and the mean local residual circulation tendency (black, contours; zero line, thick; and negative contours, dashed), in the region of the shallow circulation branch. The decadal change has been calculated as linear trend, with gray shading highlighting regions with significance level below 1 σ. The climatological thermal tropopause is shown as white line.

circulation and mixing effects. The local residual circulation effect, which generally decreases AoA in this region, becomes strongest during late winter and spring. The mixing effect increases AoA during most of the year but becomes negative in summer and hence amplifies the summertime AoA decrease.

Consideration of the decadal changes in residual circulation and mixing tendencies (Figure 7d (bottom), dashed line shows linear regression fits) shows that the circulation effect has strengthened (i.e., becoming more negative), whereas the mixing effect has remained almost unchanged for the period under consideration. This behavior is different compared to the subtropical stratosphere at higher altitudes (Figure 7b), where changes in both effects are similarly strong. Further discussion of these changes of the local effects will be provided in section 5. Note that in the lowermost stratosphere the calculated budget is less well closed compared to higher levels (black and orange lines in Figure 7d, middle) indicating that some processes are less well captured in the zonal mean budget calculation in this region (e.g., small-scale mixing).

5. Discussion

Interpreting mean age long-term changes simply in terms of changes in the local residual circulation and eddy mixing effects can be misleading, because the mean age of a given air parcel results as the integrated effect of the various tendency contributions in equation (2) along the parcel trajectory through the stratosphere (see section 3.2). However, investigation of the changes in the local effects may provide further insight into the processes locally causing these changes.

The residual circulation tendency (analogous to Figure 5) and its change during the last decade (2002–2013) in the upper troposphere and lower stratosphere is shown in Figure 8. Between about 40°N/S, the local residual circulation effect (black contours) is negative, indicating that upward and poleward advection of young air by the shallow residual circulation branch decreases mean age in this region (see also Figure 5). The significant negative decadal changes of the residual circulation effect on AoA around the tropopause (bluish shading) indicate a strengthening advection of young air by the shallow circulation branch over the last decade (note that mean age in the model was defined with respect to the boundary layer and therefore is well defined in the troposphere). This strengthening of the lowermost part of the shallow circulation branch, recently termed the "transition branch" by *Lin and Fu* [2013], is also observable in the tropical upward mass flux, which is frequently used as a measure for the strength of the residual circulation. Figure 9 shows the deseasonalized upward mass flux for the 2002–2013 period at two particular levels in the lower stratosphere, calculated from the ERA-Interim TEM vertical velocity $\overline{w}^*$ [e.g., *Andrews et al.*, 1987] between turnaround latitudes [e.g., *Seviour et al.*,

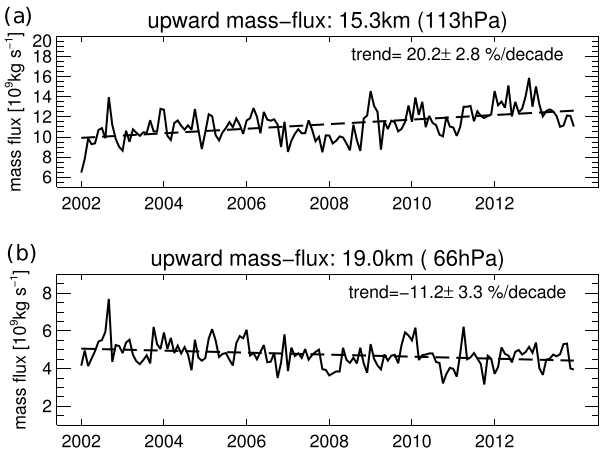

Figure 9. Tropical upward mass flux (deseasonalized) for 2002–2013 at (a) 15.3 km and (b) 19 km, calculated from ERA-Interim residual circulation upwelling between turnaround latitudes. Dashed lines show the linear fits with trend values ($\pm 1\ \sigma$ uncertainty) given in the plot.

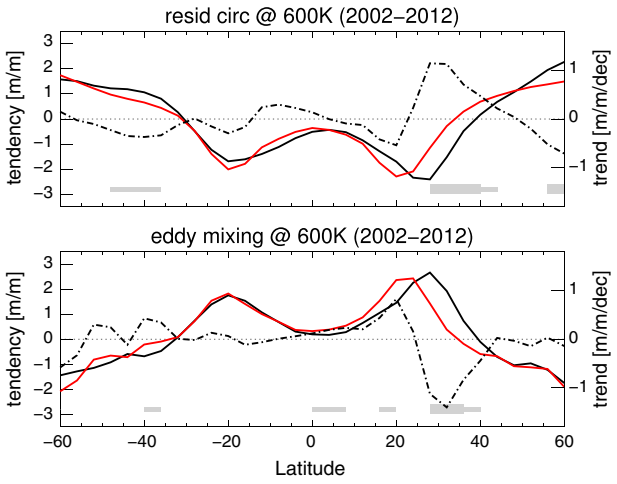

Figure 10. Latitude profiles of AoA (top) residual circulation tendency and (bottom) eddy mixing tendency at 600 K for 2002–2012. Solid lines show the tendencies, dashed lines their decadal changes (calculated as linear trends in month/month per decade). The black lines show the tendencies from the linear fit at the beginning of the 2002–2012 period, the red lines, at the end of the period (hence, the difference shows the decadal change). Thick (thin) gray lines highlight the range where trends are significant at the 2(1) σ level.

2011]. At the lower level (15.3 km) the upward mass flux has increased during the last decade, reflecting the fact of a strengthening residual circulation effect on mean age around the tropopause (Figure 8). This implies a strengthening of the shallow circulation branch, reported here for the period 2002–2013, which is in agreement with recently published analyses of mean age of air and of tropical upwelling [e.g., *Bönisch et al.*, 2011; *Garny et al.*, 2011]. At the upper level (19 km), on the contrary, the upward mass flux has decreased (Figure 9). Likewise, the local residual circulation effect causes an AoA increase (Figure 8). Consequently, our analysis shows that during the last decade the shallow residual circulation branch has accelerated only in the lowest part of the stratosphere at levels around the tropopause, in agreement with the results of *Aschmann et al.* [2014].

Figure 10 shows latitude profiles of the local residual circulation (top) and eddy mixing (bottom) effects on AoA, and their respective decadal changes (dashed), calculated from a linear regression, in the lower stratosphere at 600 K. The clearest signal is a positive decadal change in the local residual circulation effect and a negative change in the local mixing effect around 30°N. As the mean circulation tendency (solid lines) in this region is negative and the mean mixing tendency is positive, these changes represent a weakening of both effects in this region during the last decade. The black solid lines in Figure 10 show the local effects at the beginning of the decade (2002), whereas the red lines show the local effects at the end of the decade (during 2013), both calculated from the linear regression. Hence, the differences between the red and black solid lines show the decadal change during 2002–2013. Clearly, the particular change pattern implies a southward shift of the local residual circulation and mixing effect patterns over time. Note that the decadal changes (calculated from a linear regression) are significant at the 2 σ level only around their maxima (highlighted in gray). But the change patterns in both effects are very clear and related, providing additional reliability in the interpretation of a southward shift of the mean circulation pattern in the NH during the last decade. A corresponding shift in subtropical mixing barriers and implications for mean age and trace gas distributions is proposed by *Stiller et al.* [2013].

Recently, *Gerber* [2012] showed evidence for different driving mechanisms of the shallow and deep residual circulation branches. They showed from an idealized GCM study that the shallow circulation branch is mainly ("tropospherically") controlled, directly by waves caused by orography. The deep circulation branch, on the contrary, turned out to be mainly controlled by ("stratospheric") diabatic forcing of the polar vortex, which modulates wave propagation. The strong gradients in the effects of residual circulation and eddy mixing (Figure 5) support these ideas concerning a transition between different dynamical regimes (compare section 3.1). Likewise, the fact that mean age and the local circulation and mixing effects evolve differently in the lowest part of the stratosphere (below about 450 K) compared to the region above may indicate different driving mechanisms to be involved.

Clearly, the usage of reanalysis data for estimating changes on longer timescales, as done in this study regarding decadal changes, raises questions about uncertainties of the results. On the one hand, potential inhomogeneities in reanalysis data sets caused by changes in the data assimilation may introduce discontinuities into the simulation. Stratospheric temperatures in ERA-Interim reanalysis, for instance, are affected by the introduction of AMSU-A data in 1998 and radio occultation data at the end of 2006 [*Dee et al.*, 2011]. On the other hand, studies based on older reanalysis products than ERA-Interim [e.g., *Schoeberl et al.*, 2003] showed that winds from data assimilation systems may cause excessive dispersion and spurious transport

in both the vertical and horizontal direction. Furthermore, *Tan et al.* [2004] showed that this spurious subtropical transport is related to the proliferation of eddy features in the subtropics of a data assimilation system. We cannot rule out that our simulation is influenced to a certain extent by such problems. However, *Fueglistaler et al.* [2009] showed that the biases in the heat and momentum budget of ERA-Interim are much reduced compared to previous reanalysis like ERA-40. Moreover, *Monge-Sanz et al.* [2012] found recently that also the spurious dispersive transport in ERA-Interim is significantly reduced and characteristics of stratospheric transport (e.g., age of air, vertical dispersion) are clearly improved. Hence, these studies indicate a significant improvement of stratospheric transport in ERA-Interim compared to previous reanalyses.

In addition, our detailed comparison to mean age observations from MIPAS and different in situ instruments (see also Appendix A) shows that the transport model CLaMS based on ERA-Interim reanalysis data simulates stratospheric mean age of air well and even its interannual variability and change during the last decade. Although we cannot rule out biases introduced by the underlying data assimilation system, we consider this good agreement between the AoA model simulation and observations as a strong motivation for the analysis presented here. The particular AoA decadal change pattern, with increasing/decreasing AoA in the NH/SH at altitudes of the tropical pipe, is also evident to some degree from the simulations of *Diallo et al.* [2012] and *Monge-Sanz et al.* [2012], which are both based on ERA-Interim reanalysis as well, although for different time periods. All of these ERA-Interim-based AoA simulations bear resemblance to observed systematic (linear) AoA changes. Therefore, it appears useful to consider reanalysis-based estimates of these AoA changes, keeping in mind the potential biases mentioned above.

6. Summary and Conclusions

In this paper we analyzed the variability of stratospheric mean age of air (AoA) simulated with the Lagrangian chemistry transport model CLaMS for the period 1988–2013, driven by ERA-Interim winds and diabatic heating rates. We compared the model results to global AoA observations from the MIPAS instrument. Overall we found good agreement between simulated and observed AoA, even for its interannual variability and change during the last decade. In spite of the known limitations of reanalyses for trend studies (compare section 5), this underlines the usefulness of ERA-Interim-based transport simulations for analyzing interannual variability and long-term changes. In particular, the decadal AoA change during 2002–2012 from the CLaMS simulation shows reliable agreement with MIPAS observations, regarding the main significant characteristics like decreasing AoA in the SH and increasing AoA in the NH, and decreasing AoA in the lowest part of the stratosphere (below about 450 K).

We further find that AoA in the lower stratosphere shows a large interannual variability, strongly affected by the QBO. The related interannual AoA anomalies show year-to-year changes frequently of about 0.5 year, and with the QBO-induced signal clearly visible even at high latitudes. This large interannual variability emphasizes the need for continuous time series of observationally based AoA for estimating AoA variability and changes. Furthermore, it raises questions about the reliability of AoA simulations from models without a QBO. In particular, uncertainties in the representation of the QBO in models, related to the prominent role of gravity waves in driving the QBO [e.g., *Ern et al.*, 2014], may cause uncertainties in simulating interannual mean age variability.

Applying the isentropic zonal mean continuity equation to mean age allows separation of the local effects of the residual circulation and eddy mixing on AoA. The mean age at a given location results as the sum of the residual circulation transit time and of the effect of local mixing integrated along the air parcel pathway. We calculated this integrated mixing effect within the isentropic zonal mean framework and found good agreement with the recently proposed "aging by mixing" [*Garny et al.*, 2014]. In addition, our approach provides the local mixing effect at every location and time in the atmosphere.

The comparison of these local effects of circulation and mixing on AoA shows that both local effects are largely opposite and of the same order of magnitude. Therefore, AoA changes are the result of a delicate local balance between the competing effects of residual circulation and mixing. Consequently, AoA changes are not unambiguously related to residual circulation changes, and diagnosing circulation changes from AoA without accounting for mixing effects seems problematic, in general.

The local mixing effect is strongest in the lower stratosphere below about 500 K (~20 km); hence, mixing mainly occurs below this level. However, mixing impacts AoA at all levels above, as pointed out by *Garny*

et al. [2014]. In particular, local mixing increases AoA in the tropics equatorward of about 40° by mixing in aged air from higher latitudes and decreases AoA poleward, by exchange of air with the tropics. The local effect of the residual circulation is a mirror image of the mixing effect, decreasing AoA at low latitudes and increasing AoA at high latitudes. The strong vertical gradients of local mixing and circulation effects around 500 K, as well as the strong horizontal gradients around 40°N/S are consistent with the existence of a deep and a shallow residual circulation branch, as proposed by *Birner and Bönisch* [2011].

In the lowest part of the stratosphere, the local residual circulation effect strengthened during the last decade (2002–2012). We interpret this decadal change as a strengthening of the shallow residual circulation branch, supporting the results of *Birner and Bönisch* [2011] and *Bönisch et al.* [2011]. In the lower stratosphere above, at levels of the tropical pipe, the decadal changes of the local mixing and circulation effects are related and can be interpreted as a southward shift of the mean circulation pattern. This interpretation supports the hypothesis of a southward shift of the subtropical mixing barriers during the last decade [*Stiller et al.*, 2013] as reason for the observed decadal AoA and trace gas changes.

Appendix A: Comparison of Simulated Mean Age to Observations

In addition to MIPAS satellite observations, further AoA estimates exist based on airborne in situ observations of SF_6 and CO_2, from different measurement campaigns during the last decades. This AoA data set has been used in several studies as a standard benchmark for validation of model simulations [e.g., *Waugh and Hall*, 2002]. For completeness, we compare the CLaMS simulated mean age of air with this data set.

Figure A1 compares latitudinal profiles of CLaMS simulated mean age of air at 20 km, AoA based on MIPAS observations of SF_6 [*Haenel et al.*, 2014] and on airborne in situ observations of SF_6 and CO_2 (same data as shown in *Waugh and Hall* [2002], based on various measurements, [*Boering et al.*, 1996; *Andrews et al.*, 2001; *Elkins et al.*, 1996; *Ray et al.*, 1999; *Harnisch et al.*, 1996]). The shadings show the range of monthly mean values for CLaMS and MIPAS, while the error bars show the range between minimum and maximum in situ observations in each latitude bin. Overall, the agreement between CLaMS and in situ CO_2-based AoA is very good. Compared to SF_6-based estimates, CLaMS shows younger age particularly at high latitudes, likely related to the mesospheric sink of SF_6. In middle latitudes, simulated AoA is at the lower end of the observational range. Further, in the subtropics, the simulated AoA gradient appears slightly weaker than observed in situ, but agrees with the latitudinal gradient from MIPAS. However, all these differences between simulated and observed AoA are similar in magnitude to the differences between AoA from the different observational sources. We conclude that CLaMS simulated AoA at 20 km reliably agrees with the range covered by the different in situ and satellite observations.

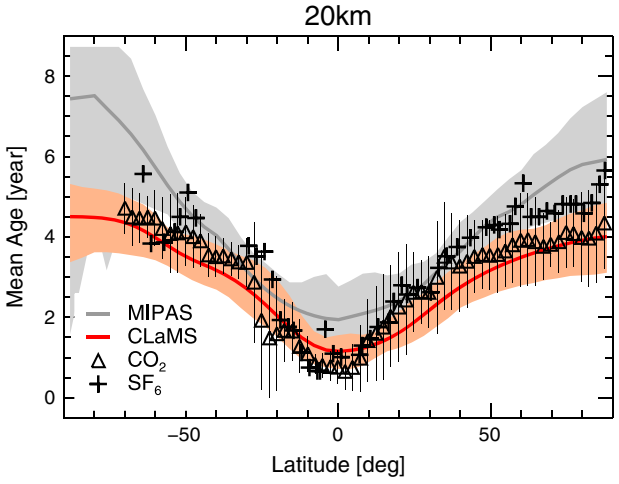

Figure A1. Zonal mean age of air profiles at 20 km from CLaMS simulation (red), MIPAS satellite observations (gray), both for 2002–2012, and from in situ observations of CO_2 and SF_6 (symbols). Shadings show the range of monthly mean values for CLaMS and MIPAS observations. Error bars show the range between maximum and minimum in situ observations in each latitude bin.

Appendix B: Vertical and Horizontal Residual Circulation and Mixing Tendencies

Figure B1 shows the local residual circulation and mixing tendencies in the mean age budget equation (2), similar to Figure 5 but separated into their vertical and horizontal components. Clearly, the residual circulation tendency is dominated by its vertical component. Only at subtropical latitudes, around the edge of the tropical pipe, horizontal advection by the residual circulation also contributes. This horizontal contribution decreases AoA by poleward advection of young tropical air. The mixing tendency, on the other hand, is dominated by its

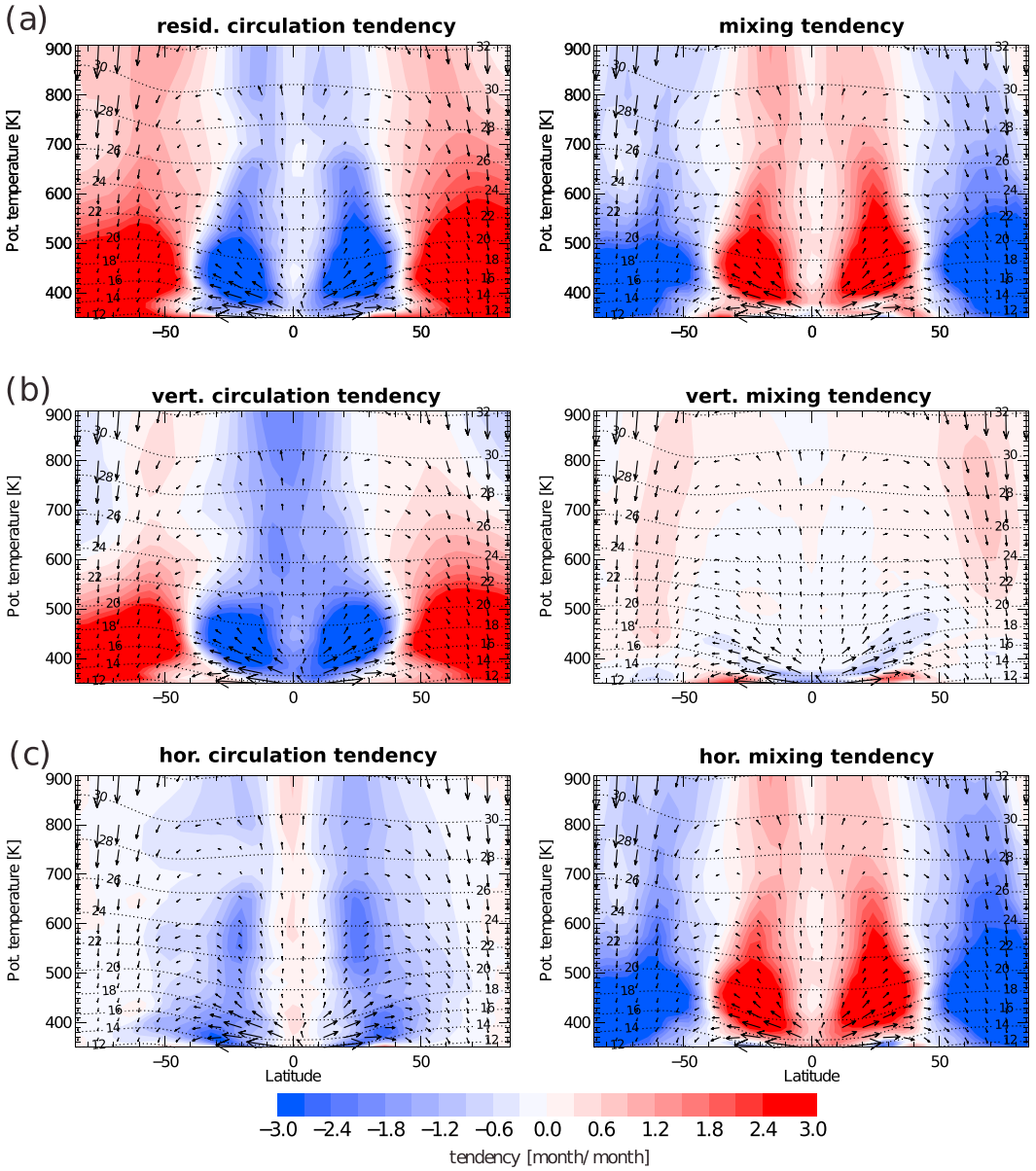

Figure B1. Contributions of (left) residual circulation and (right) eddy mixing to the mean age tendency budget, as 2002–2012 average, deduced from the isentropic AoA continuity equation (2). The (a) full tendencies, (b) their vertical components, and (c) their horizontal components. Altitude levels are shown as dashed, residual circulation as arrows.

horizontal component, reflecting the isentropic (quasi-horizontal) nature of eddy mixing. As eddy mixing exchanges air masses in a two-way process, it increases AoA at low latitudes and decreases AoA at latitudes poleward of about 40°N/S.

Acknowledgments
We thank Thomas Birner for comments on an earlier version of the manuscript, Manfred Ern, Marta Abalos, and Bernard Legras for helpful discussions, Nicole Thomas for excellent programming support, and the ECMWF for providing reanalysis data. Felix Ploeger was supported by a postdoc grant of the Helmholtz association. The CLaMS model data may be requested from the corresponding author (f.ploeger@fz-juelich.de).

References

Abalos, M., F. Ploeger, P. Konopka, W. J. Randel, and E. Serrano (2013a), Ozone seasonality above the tropical tropopause: Reconciling the Eulerian and Lagrangian perspectives of transport processes, *Atmos. Chem. Phys.*, *13*, 10,787–10,794.

Abalos, M., W. J. Randel, D. E. Kinnison, and E. Serrano (2013b), Quantifying tracer transport in the tropical lower stratosphere using WACCM, *Atmos. Chem. Phys.*, *13*, 10,591–10,607.

Andrews, A. E., et al. (2001), Mean ages of stratospheric air derived from in situ observations of CO_2, CH_4, and N_2O, *J. Geophys. Res.*, *106*, 32,295–32,314.

Andrews, D. G., J. R. Holton, and C. B. Leovy (1987), *Middle Atmosphere Dynamics*, Acad. Press, San Diego, Calif.

Aschmann, J., J. P. Burrows, C. Gebhardt, A. Rozanov, R. Hommel, M. Weber, and A. M. Thompson (2014), On the hiatus in the acceleration of tropical upwelling since the beginning of the 21st century, *Atmos. Chem. Phys.*, *14*, 12,803–12,814.

Baldwin, M. P., et al. (2001), The quasi-biennial oscillation, *Rev. Geophys.*, *39*, 179–229, doi:10.1029/1999RG000073.

Birner, T., and H. Bönisch (2011), Residual circulation trajectories and transit times into the extratropical lowermost stratosphere, *Atmos. Chem. Phys.*, *11*, 817–827, doi:10.5194/acp-11-817-2011.

Boering, K. A., S. C. Wofsy, B. C. Daube, H. R. Schneider, M. Loewenstein, J. R. Podolske, and T. J. Conway (1996), Stratospheric mean ages and transport rates from observations of carbon dioxide and nitrous oxide, *Science*, *274*, 1340–1343.

Bönisch, H., A. Engel, J. Curtius, T. Birner, and P. Hoor (2008), Quantifying transport into the lowermost stratosphere using simultaneous in-situ measurements of SF_6 and CO_2, *Atmos. Chem. Phys.*, *10*, 5905–5919.

Bönisch, H., A. Engel, T. Birner, P. Hoor, D. W. Tarasick, and E. A. Ray (2011), On the structural changes in the Brewer-Dobson circulation after 2000, *Atmos. Chem. Phys.*, *11*, 3937–3948, doi:10.5194/acp-11-3937-2011.

Brewer, A. W. (1949), Evidence for a world circulation provided by the measurements of helium and water vapour distribution in the stratosphere, *Q. J. R. Meteorol. Soc.*, *75*, 351–363.

Butchart, N., et al. (2010), Chemistry-climate model simulations of twenty-first century stratospheric climate and circulation changes, *J. Clim.*, *23*, 5349–5374, doi:10.1175/2010JCLI3404.1.

Choi, W., H. Lee, W. B. Grant, J. H. Park, J. H. Holton, K.-M. Lee, and B. Naujokat (2002), On the secondary meridional circulation associated with the quasi-biennial oscillation, *Tellus*, *54B*, 395–406.

Dee, D. P., et al. (2011), The ERA-interim reanalysis: Configuration and performance of the data assimilation system, *Q. J. R. Meteorol. Soc.*, *137*, 553–597, doi:10.1002/qj.828.

Diallo, M., B. Legras, and A. Chedin (2012), Age of stratospheric air in the ERA-Interim, *Atmos. Chem. Phys.*, *12*, 12,133–12,154.

Dobson, G. M. B., D. N. Harrison, and J. Lawrence (1929), Measurements of the amount of ozone in the Earth's atmosphere and its relation to other geophysical conditions. Part III, *Proc. R. Soc. London A*, *122*, 456–486.

Elkins, J. W., et al. (1996), Airborne gas chromatograph for in situ measurements of long-lived species in the upper troposphere and lower stratosphere, *Geophys. Res. Lett.*, *23*(4), 347–350, doi:10.1029/96GL00244.

Engel, A., et al. (2009), Age of stratospheric air unchanged within uncertainties over the past 30 years, *Nature*, *2*, 28–31, doi:10.1038/ngeo388.

Ern, M., F. Ploeger, P. Preusse, J. C. Gille, L. J. Gray, S. Kalisch, M. G. Mlynczak, J. M. Russell III, and M. Riese (2014), Interaction of gravity waves with the QBO: A satellite perspective, *J. Geophys. Res. Atmos.*, *119*, 2329–2355, doi:10.1002/2013JD020731.

Fueglistaler, S., B. Legras, A. Beljaars, J. J. Morcrette, A. Simmons, A. M. Tompkins, and S. Uppala (2009), The diabatic heat budget of the upper troposphere and lower/mid stratosphere in ECMWF reanalysis, *Q. J. R. Meteorol. Soc.*, *135*, 21–37, doi:10.1002/qj.361.

Garcia, R. R., and W. J. Randel (2008), Acceleration of Brewer-Dobson circulation due to increase in greenhouse gases, *J. Atmos. Sci.*, *65*, 2731–2739.

Garcia, R. R., W. J. Randel, and E. D. Kinnison (2011), On the determination of age of air trends from atmospheric trace species, *J. Atmos. Sci.*, *68*, 139–154.

Garny, H., M. Dameris, W. J. Randel, G. E. Bodeker, and R. Deckert (2011), Dynamically forced increase of tropical upwelling in the lower stratosphere, *J. Atmos. Sci.*, *68*, 1214–1233, doi:10.1175/2011JAS3701.1.

Garny, H., T. Birner, H. Bönisch, and F. Bunzel (2014), The effects of mixing on age of air, *J. Geophys. Res. Atmos.*, *119*, 7015–7034, doi:10.1002/2013JD021417.

Gerber, E. P. (2012), Stratospheric versus tropospheric control of the strength and structure of the Brewer-Dobson circulation, *J. Atmos. Sci.*, *69*, 2857–2877.

Gray, L. J., and J. M. Russell III (1999), Interannual variability of trace gases in the subtropical winter stratosphere, *J. Atmos. Sci.*, *56*, 977–993.

Haenel, F., G. Stiller, T. von Clarmann, B. Funke, N. Glatthor, U. Grabowski, S. Kellmann, M. Kiefer, and A. Linden (2014), Improved SF_6 and age of stratospheric air data from MIPAS, *EGU General Assembly*, Geophys. Res. Abstr., 16, EGU2014-12998, Vienna, Austria, 27 April - 2 May.

Hall, T. M., and R. A. Plumb (1994), Age as a diagnostic of stratospheric transport, *J. Geophys. Res.*, *99*(D1), 1059–1070.

Harnisch, J., R. Borchers, P. Fabian, and M. Maiss (1996), Tropospheric trends for CF_4 and C_2F_6 since 1982 derived from SF_6 dated stratospheric air, *Geophys. Res. Lett.*, *23*(10), 1099–1102, doi:10.1029/96GL01198.

Haynes, P., and E. Shuckburgh (2000a), Effective diffusivity as a diagnostic of atmospheric transport 1. Stratosphere, *J. Geophys. Res.*, *105*, 22,777–22,794.

Haynes, P., and E. Shuckburgh (2000b), Effective diffusivity as a diagnostic of atmospheric transport 2. Troposphere and lower stratosphere, *J. Geophys. Res.*, *105*(D18), 22,795–22,810.

Haynes, P., C. J. Marks, M. E. McIntyre, T. G. Shepherd, and K. P. Shine (1991), On the downward control of extratropical diabatic circulations by eddy-induced mean zonal forces, *J. Atmos. Sci.*, *48*, 651–679.

Holton, J. R., and H.-C. Tan (1980), The influence of the equatorial quasi-biennial oscillation on the global circulation at 50 mb, *J. Atmos. Sci.*, *37*, 2200–2208.

Konopka, P., et al. (2004), Mixing and ozone loss in the 1999–2000 Arctic vortex: Simulations with the 3-dimensional Chemical Lagrangian Model of the Stratosphere (CLaMS), *J. Geophys. Res.*, *109*, D02315, doi:10.1029/2003JD003792.

Konopka, P., J. U. Grooß, G. Günther, F. Ploeger, R. Pommrich, R. Müller, and N. Livesey (2010), Annual cycle of ozone at and above the tropical tropopause: Observations versus simulations with the Chemical Lagrangian Model of the Stratosphere (CLaMS), *Atmos. Chem. Phys.*, *10*, 121–132.

Lin, P., and Q. Fu (2013), Changes in various branches of the Brewer-Dobson circulation from an ensemble of chemistry climate models, *J. Geophys. Res. Atmos.*, *118*, 73–84, doi:10.1029/2012JD018813.

McKenna, D. S., P. Konopka, J.-U. Grooß, G. Günther, R. Müller, R. Spang, D. Offermann, and Y. Orsolini (2002), A new Chemical Lagrangian Model of the Stratosphere (CLaMS): 1. Formulation of advection and mixing, *J. Geophys. Res.*, *107*(D16), 4309, doi:10.1029/2000JD000114.

Monge-Sanz, B. M., M. P. Chipperfield, D. P. Dee, A. J. Simmons, and S. M. Uppala (2012), Improvements in the stratospheric transport achieved by a chemistry transport model with ECMWF (re)analyses: Identifying effects and remaining challenges, *Q. J. R. Meteorol. Soc.*, *139*, 654–673.

Neu, L. L., and R. A. Plumb (1999), Age of air in a "leaky pipe"ž model of stratospheric transport, *J. Geophys. Res.*, *104*(D16), 19,243–19,255.

Newman, P. A., and E. R. Nash (2006), The unusual Southern Hemisphere stratosphere winter of 2002, *J. Atmos. Sci.*, *62*(3), 614–628.

Oberländer, S., U. Langematz, and S. Meul (2013), Unraveling impact factors for future changes in the Brewer-Dobson circulation, *J. Geophys. Res. Atmos.*, *118*, 10,296–10,312, doi:10.1002/jgrd.50775.

Palazzi, E., F. Fierli, G. P. Stiller, and J. Urban (2011), Probability density functions of long-lived tracer observations from satellite in the subtropical barrier region: Data intercomparison, *Atmos. Chem. Phys.*, *11*, 10,579–10,598, doi:10.5194/acp-11-10579-2011.

Ploeger, F., P. Konopka, G. Günther, J.-U. Grooß, and R. Müller (2010), Impact of the vertical velocity scheme on modeling transport in the tropical tropopause layer, *J. Geophys. Res.*, *115*, D03301, doi:10.1029/2009JD012023.

Ploeger, F., G. Günther, P. Konopka, S. Fueglistaler, R. Müller, C. Hoppe, A. Kunz, R. Spang, J.-U. Grooß, and M. Riese (2013), Horizontal water vapor transport in the lower stratosphere from subtropics to high latitudes during boreal summer, *J. Geophys. Res. Atmos.*, *118*, 8111–8127, doi:10.1002/jgrd.5063.

Plumb, R. A. (1996), A "tropical pipe" model of stratospheric transport, *J. Geophys. Res.*, *101*, 3957–3972.

Plumb, R. A. (2002), Stratospheric transport, *J. Meteorol. Soc. Jpn.*, *80*(4B), 793–809.

Pommrich, R., et al. (2014), Tropical troposphere to stratosphere transport of carbon monoxide and long-lived trace species in the Chemical Lagrangian Model of the Stratosphere (CLaMS), *Geosci. Model Dev. Discuss.*, *7*, 5087–5139, doi:10.5194/gmdd-7-5087-2014.

Punge, H. J., P. Konopka, M. A. Giorgetta, and R. Müller (2009), Effects of the quasi-biennial oscillation on low-latitude transport in the stratosphere derived from trajectory calculations, *J. Geophys. Res.*, *114*, D03102, doi:10.1029/2008JD010518.

Randel, W. J., B. A. Boville, J. C. Gille, P. L. Bailey, S. T. Massie, J. B. Kumer, J. L. Mergenthaler, and A. E. Roche (1994), Simulation of stratospheric N_2O in the NCAR CCM2: Comparison with CLAES data and global budget analyses, *J. Atmos. Sci.*, *51*(20), 2834–2845.

Randel, W. J., F. Wu, J. M. Russell, A. Roche, and J. W. Waters (1998), Seasonal cycles and QBO variations in stratospheric CH_4 and H_2O observed in UARS HALOE data, *J. Atmos. Sci.*, *55*(2), 163–185.

Ray, E. A., F. L. Moore, J. W. Elkins, G. S. Dutton, D. W. Fahey, H. Vömel, S. Oltmans, and K. H. Rosenlof (1999), Transport into the Northern Hemisphere lowermost stratosphere revealed by in situ tracer measurements, *J. Geophys. Res.*, *104*, 26,565–26,580.

Ray, E. A., et al. (2010), Evidence for changes in stratospheric transport and mixing over the past three decades based on multiple data sets and tropical leaky pipe analysis, *J. Geophys. Res.*, *115*, D21304, doi:10.1029/2010JD014206.

Riese, M., F. Ploeger, A. Rap, B. Vogel, P. Konopka, M. Dameris, and P. M. Forster (2012), Impact of uncertainties in atmospheric mixing on simulated UTLS composition and related radiative effects, *J. Geophys. Res.*, *117*, D16305, doi:10.1029/2012JD017751.

Rind, D., R. Suozzo, N. K. Balachandran, and M. J. Prather (1990), Climate change and the middle atmosphere. Part I: The doubled CO_2 climate, *J. Atmos. Sci.*, *47*, 475–494.

Schoeberl, M. R., A. R. Douglass, Z. X. Zhu, and S. Pawson (2003), A comparison of the lower stratospheric age spectra derived from a general circulation model and two data assimilation systems, *J. Geophys. Res.*, *108*(D3), 4113, doi:10.1029/2002JD002652.

Seviour, W. J. M., N. Butchart, and S. C. Hardiman (2011), The Brewer-Dobson circulation inferred from ERA-Interim, *Q. J. R. Meteorol. Soc.*, *138*, 878–888.

Shepherd, T. G., and C. McLandress (2011), A robust mechanism for strengthening of the Brewer-Dobson circulation in response to climate change: Critical-layer control of subtropical wave breaking, *J. Atmos. Sci.*, *68*, 784–797, doi:10.1175/2010JAS3608.1.

Shuckburgh, E., W. Norton, A. Iwi, and P. Haynes (2001), The influence of the quasi-bienniel oscillation on isentropic transport and mixing in the tropics and subtropics, *J. Geophys. Res.*, *106*, 14,327–14,338.

Solomon, S., K. H. Rosenlof, R. W. Portmann, J. Daniel, S. M. Davis, T. J. Sanford, and G. K. Plattner (2010), Contributions of stratospheric water vapor to decadal changes in the rate of global warming, *Science*, *327*, 1219–1223.

SPARC-CCMVal (2010), SPARC report on the evaluation of chemistry-climate models, *Tech. Rep., SPARC Rep. 5, WCRP-132, WMO/TD-1526*, edited by V. Eyring, T. G. Shepherd, and D. W. Waugh.

Sparling, L. C. (2000), Statistical perspectives on stratospheric transport, *Rev. Geophys.*, *38*(4), 417–436.

Stiller, G. P., et al. (2008), Global distribution of mean age of stratospheric air from MIPAS SF_6 measurements, *Atmos. Chem. Phys.*, *8*(3), 677–695.

Stiller, G. P., et al. (2012), Observed temporal evolution of global mean age of stratospheric air for the 2002 to 2010 period, *Atmos. Chem. Phys.*, *12*, 3311–3331.

Stiller, G. P., F. Fierli, T. von Clarmann, B. Funke, and T. Reddmann (2013), Can the MIPAS-observed pattern of mean age of air trends be explained by shifts of the subtropical mixing barriers?, Abstract A23F-0338 presented at 2013 Fall Meeting, AGU, San Francisco, Calif.

Strahan, S. E., M. R. Schoeberl, and S. D. Steenrod (2009), The impact of tropical recirculation of polar composition, *Atmos. Chem. Phys.*, *9*, 2471–2480.

Tan, W. W., M. A. Geller, S. Pawson, and A. da Silva (2004), A case study of excessive subtropical transport in the stratosphere of a data assimilation system, *J. Geophys. Res.*, *109*, D11102, doi:10.1029/2003JD004057.

Waugh, D. W. (2009), The age of stratospheric air, *Nature*, *2*, 14–16.

Waugh, D. W., and T. M. Hall (2002), Age of stratospheric air: Theory, observations, and models, *Rev. Geophys.*, *40*(4), 1010, doi:10.1029/2000RG000101.